Paleomagnetic and paleoclimatic investigation at Laguna Melincue (Pampean Plains, Argentina): preliminary results

ROMINA V. ACHAGA[1], MARIA A. IRURZUN[1], CLAUDIA S.G. GOGORZA[1], AVTO GOGUITCHAICHVILI[2], JUAN MORALES[2], DANIEL LOPONTE[3] AND ANA M. SINITO[1]

1 Centro de Investigaciones en Fisica e Ingenieria del Centro de la Provincia de Buenos Aires (CIFICEN), UNCPBA-CONICET-CICPBA, Tandil, Argentina (romi.achaga@gmail.com)

2 Instituto de Geofisica, Unidad Michoacan, Universidad Nacional Autonoma de Mexico, Campus Morelia, 58190 Morelia, Mexico

3 Instituto Nacional de Antropologia y Pensamiento Latinoamericano, Ciudad Autonoma de Buenos Aires, Argentina

Received: June 1, 2016; Revised: Septemebr 12, 2016; Accepted: November 30, 2016

ABSTRACT

Laguna Melincué is a shallow lake located in Santa Fe Province, Argentina (33°41'27.8"S, 61°31'36.5"W). The catchment area is around 1495 km^2 and it is located in the Pampean Plains. It was reduced to 678 km^2 by the construction of the San Urbano channel in 1941 and reconditioned in 1977, which was built to avoid floods. The floods are related to some El Niño episodes, with high precipitation events. The lake has been previously studied from different approaches, mainly to understand hydrological and climatic variations, but more multidisciplinary studies are needed to understand its complex hydrological situation. Here we present the first paleomagnetic and rock magnetic studies made on a short sediment core collected from the lake in order to contribute to identifying paleoclimatic proxies and to present the first paleomagnetic results for the site. Rock magnetic analyses suggest that the well-preserved magnetic mineralogy is dominated by pseudo single-domain (titano)magnetite and/or maghemite. The results also indicate that a stable characteristic remanent magnetisation can be isolated and thus the directions of the geomagnetic field may be obtained, providing evidence for the use of this lake for paleomagnetic and paleoenvironmental studies. Changes in magnetic grain size and concentration of magnetic minerals suggest environmental variations and changes in the lake level, which are consistent with historical reports. The paleomagnetic results agree well with Cals3k.3 model for inclination and declination of the geomagnetic field except for the dry period probably due to the fact that the core was extracted near the shore.

Keywords: rock magnetism, magnetic grain-size, magnetic mineralogy, paleosecular variation, environmental changes

Stud. Geophys. Geod., 61 (2017), 318–335, DOI: 10.1007/s11200-016-1247-0

1. INTRODUCTION

Water bodies and their sediments are containers of diverse information. In particular, lake sediments have been widely used for paleoclimatic and paleomagnetic studies around the world (*Veski et al., 2004*; *Šroubek et al., 2007*; *Moernaut et al., 2010*; *Lise-Pronovost et al., 2013*; *Irurzun et al., 2014c*; *Lund and Platzman, 2016*). Rock magnetic studies are very useful to investigate mineralogy, concentration and grain size of the magnetic minerals contained in a sediment core (*Liu et al., 2012*; *Chaparro et al., 2014*; *Irurzun et al., 2014a*). Paleomagnetic studies are also used as tools for sediment dating and to interpret the behaviour of the Earth's geomagnetic field (*Yang et al., 2000*; *Gogorza et al., 2011*; *Irurzun et al., 2014b*). The combination of both methods leads to a better interpretation of the magnetic results obtained from lake sediments, altogether with other disciplines.

Although there are many hydrological, geochemical, paleoclimatic and geological studies on the Pampean Plains (*Biasatti et al., 1999*; *Piovano et al., 2004*; *Laprida et al., 2009*; *Brunetto et al., 2010*; *Irurzun et al., 2014a*; among others), few of them focused on Laguna Melincué. This lake is interesting to study because it shows variations in the lake level that cause flooding in the surroundings cities.

Among the few available studies, *Pasotti et al. (1984)* performed hydrological analysis and identified two subwatersheds (A and B) causing various forms of surface and groundwater runoff to lower areas. Mainly, they tried to detect the cause of an uncontrolled rise of the lake level and suggested an interdisciplinary approach to solve the problem and to perform sediment analysis. *Guerra et al. (2015)* carried out paleoclimatic studies on two short sediment cores in this lake. They found three sedimentary units representing different environmental conditions. Unit C including Medieval Climatic Anomaly (MCA) and Little Ice Age (LIA) composed of massive and compact grey sediments, Unit B formed by banded organic-rich sediments with gradual declination in the lake internal productivity and raising salinities to the top of the unit and Unit A composed of organic-rich and fine silts sets.

2. SITE DESCRIPTION

Laguna Melincué (Fig. 1) is a shallow lake (approximately 4 m in depth in 2014) located in Santa Fe Province, Argentina (33°41′27.8″S, 61°31′36.5″W). The catchment area is around 1495 km^2 and it is located in the Pampean Plains. It was reduced to 678 km^2 by the construction of the San Urbano channel in 1941 and reconditioned in 1977 (*melincue.gob.ar*), which was built to avoid floods. The basin is placed in a tectonically sunken block. The lake has a closed basin without important tributaries or effluents of permanent flow, and eliminated by evaporation (*Pasotti et al., 1984*). The floods are related to some El Niño episodes, with high precipitation events (*Guerra et al., 2015*; *Peralta, 2003*). In those moments, the lake water level was so high that reached Melincué city. *Pasotti et al. (1984)* show maps where the evolution of Laguna Melincué can be found.

The meteorological stations used to infer current weather conditions were Casilda, Pergamino, Junin and Laboulaye (*Pasotti et al., 1984*). The mean annual precipitation is

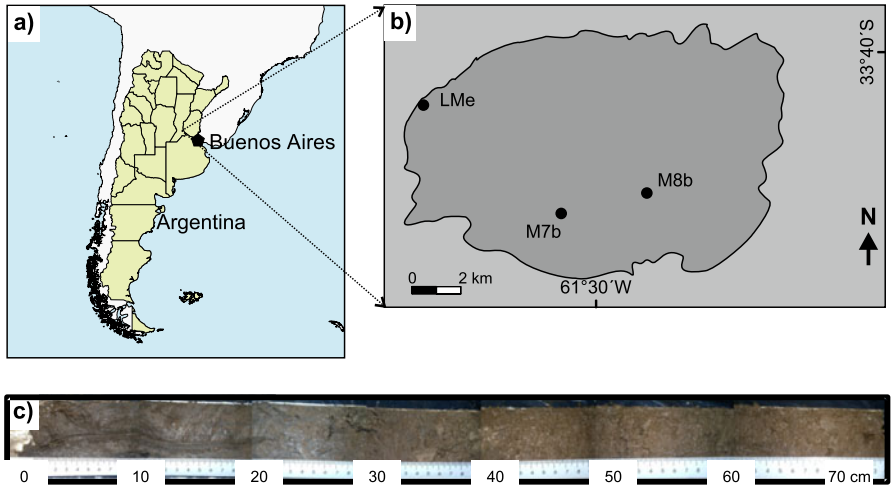

Fig. 1. **a)** Location of Laguna Melincué in the South America Pampean Plains, satellite image, **b)** drawing showing the lake with the coring sites, **c)** LMe core.

about 970 mm with the highest precipitation during austral autumn. The mean temperatures vary annually between 9.5°C and 24°C in winter and summer, respectively (*Pasotti et al., 1984*). The general description of the present day climate is temperate subhumid-humid. Laguna Melincué is situated to the NE of the Arid Diagonal (*Bruniard 1982*), which divides the Patagonian Westerlies from the South American Monsoonal system (*Guerra, et al., 2015*). The prevailing winds come from the N causing relative high humidity and temperature. The SW winds are less frequent but have high intensity and cause drier conditions and lower temperature (*Pasotti et al., 1984*).

3. MATERIAL AND METHODS

3.1. Field work and sampling

A 6-cm diameter cylindrical core LMe (length of 74 cm) was collected from the Laguna Melincué (33°41′27.8″S, 61°31′36.5″W) at a depth of 45 cm below the water level in October 2014 (Fig. 1). After the core was split lengthwise and described, it was stored in a cool room at 4°C. In the laboratory, the LMe core was sub-sampled continuously with cubic plastic boxes ($20 \times 20 \times 20$ mm) that were pushed into the surface of the open core face. A total of 32 samples were obtained for paleomagnetic and rock magnetic analysis.

3.2. Methods

A set of laboratory experiments were carried out on every sample of LMe to obtain a magnetic characterisation of the sediments. Volume magnetic susceptibility (k) was measured using a Bartington MS3 point sensor every 0.5 cm on one half of the LMe core surface. Magnetic susceptibility of cubic specimens was measured at 0.47 kHz (k_{low}) and

4.7 kHz (k_{high}), respectively, using a Bartington MS2 Magnetic Susceptibilimeter. These values were used to calculate the relative frequency-dependent susceptibility, $F = \left(k_{low} - k_{high} \right) / k_{low}$, expressed in % (*Dearing et al., 1996*).

The intensity of the Natural Remanent Magnetization (*NRM*) and directions (declination *D* and inclination *I*) were measured using a JR6A Dual Spinner Magnetometer. The stability of the *NRM* and the directions were analysed by alternating-field (AF) demagnetization using an AF demagnetizer (Molspin Ltd.). When possible, the samples were demagnetized successively at peak fields of 5, 10, 15, 20, 25, 30, 35, 40, 50, 60, 70 and 100 mT.

The Anhysteretic Remanent Magnetization (*ARM*) was acquired in an AF peak of 100 mT and a direct current (DC) biasing field of 0.05 mT using the same AF demagnetizer with a pARM device (Molspin Ltd.). Subsequently, AF demagnetization of the *ARM* was made following the same steps as for the *NRM* demagnetization. Isothermal Remanent Magnetization (*IRM*) was acquired at room temperature in increasing steps until 1.2 T, reaching the saturation (*SIRM*) and in increasing steps in back fields until 300 mT using a IM-10-30 Pulse Magnetizer (ASC Scientific). A high direct field of 1.2 T was imparted to reach the *SIRM* value again.

Associated parameters *S* ratio ($-IRM_{-300\,mT} / SIRM$), remanent coercive field (B_{cr}), $SIRM/k$, ARM/k and $ARM/SIRM$ were calculated. The median destructive field of the *NRM* and *ARM* (MDF_{NRM} and MDF_{ARM}) were calculated in order to determine the required applied field to remove 50% of the initial remanence. All remanent magnetizations were measured with a JR6A Dual Speed Spinner Magnetometer.

All sediment samples were measured using a Variable Field Translation Balance (Model MMVFTB) in order to obtain the hysteresis curves and derived properties, including the bulk coercive force (B_c), the remanent coercive force (B_{cr}), the saturation magnetization (M_s) and the saturation remanence (M_{rs}). The coercivity (B_{cr}/B_c) and the remanence (M_{rs}/M_s) ratios were used as parameters for a Day's plot (*Day et al., 1977*, modified by *Dunlop, 2002*). In order to further investigate the magnetic mineralogy, the temperature-dependence of magnetization (*M-T*) was measured for all core samples using the same equipment.

NRM is influenced by the intensity of the geomagnetic field at the moment of deposition and by lithological factors such as concentration, mineralogy and grain size of the magnetic carriers (*Tauxe, 1993*). While *k* and the remanent magnetic parameters (such as *ARM*, *IRM*) depend on both the concentration and the magnetic grain size; the inter-parametric ratios $SIRM/k$, ARM/k, $ARM/SIRM$, B_{cr}/B_c and M_{rs}/M_s, as well as MDF_{NRM}, are considered potential magneto-granulometric indicators, with higher values for finer grained (single-domain, SD) ferrimagnetic particles and lower values for larger (multi-domain, MD) grains (*Dunlop and Özdemir, 1997*). This assumption has been questioned for multiphase assemblages (*Anderson and Rippey, 1988*) and, therefore, interpretation of mixed sedimentary mineral assemblages should be carefully analysed. Finally, *S* ratio is used to indicate the relative concentration of low versus high coercivity minerals (*Bloemendal et al., 1992*).

4. RESULTS

4.1. Magnetic susceptibility correlation

Figure 2a,c shows the summarised information from cores M7b and M8b (Fig. 1) from *Guerra et al. (2015)* regarding the magnetic susceptibility, lithological units, sedimentation rates and worldwide climatic episodes: Little Ice Age (LIA) and Medieval Climatic Anomaly (MCA). M7b and M8b samples were dated using ^{210}Pb and ^{14}C (*Guerra et al., 2015*). Figure 2c shows the obtained *k* values measured every 0.5 cm on core LMe. The cores were correlated using magnetic susceptibility and lithological features, but for clarity only the first in shown in this work. Between tie points, sediment depths were calculated by linear interpolation. Using this correlation the chronology established by *Guerra et al. (2015)* was transferred to LMe. Since LMe core is slightly older, an extrapolated basal calibrated age of 720 yrs BP was obtained for it. The

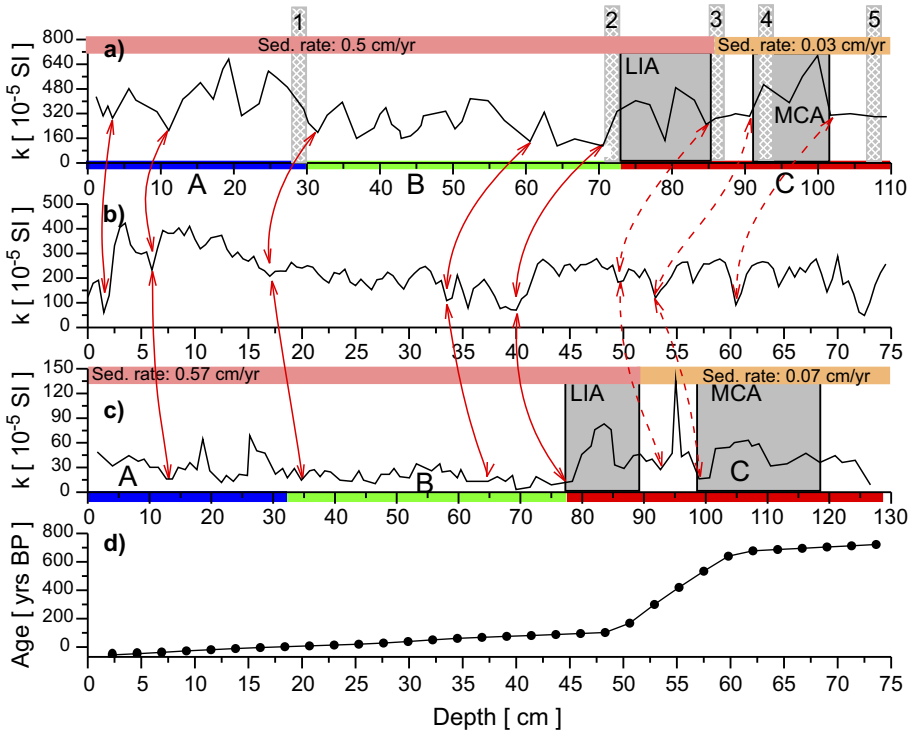

Fig. 2. Correlation lines used for calibration of core LMe. **a)** Overview of units, sedimentation rates, and climatic events of core M7b taken from *Guerra et al. (2015)*. Numbers indicate age control points (1: 1976 ± 4 AD, 2: 1878 ± 10 AD, 3: 1454 ± 48 AD, 4: 1170 ± 55 AD, 5: 806 ± 78 AD); **b)** magnetic susceptibility *k* log of core LMe; **c)** overview of units, sedimentation rates, and climatic events of core M8b taken from *Guerra et al. (2015)*; **d)** age-depth model for core LMe (depth corresponds to cubic boxes). LIA: Little Ice Age, MCA: Medieval Climatic Anomaly

extrapolation was calculated using the average sedimentation rate for core LMe from 0 to 60 cm, 0.26 cm/yr. Figure 2d shows the age-depth model obtained for LMe.

4.2. Rock magnetic analysis

The logs of *k*, *NRM*, *ARM* and *SIRM* versus age for the cubic samples are shown in Fig. 3. They display similar characteristics with correspondence in peaks and troughs, which clearly illustrates the influence of the magnetic concentration and grain size on the *NRM*, as expected for a magnetic mineralogy dominated by magnetite (*Lisé-Pronovost et al., 2012*). Magnetic susceptibility oscillates between 113×10^{-5} and 393×10^{-5} SI with a mean value of 271.5×10^{-5} SI for Unit A, 166.8×10^{-5} SI for Unit B and 199.4×10^{-5} SI for Unit C. The mean values of *NRM*, *ARM* and *SIRM* are, respectively, 81.5 mA/m, 1285.5 mA/m and 44.9 A/m for Unit A; 41.6 mA/m, 556.3 mA/m and 25.2 mA/m for Unit B; and 33.5 mA/m, 695.1 mA/m and 38.1 A/m for Unit C. The most notable rock-magnetic change is a sharp increase in the concentration of magnetic

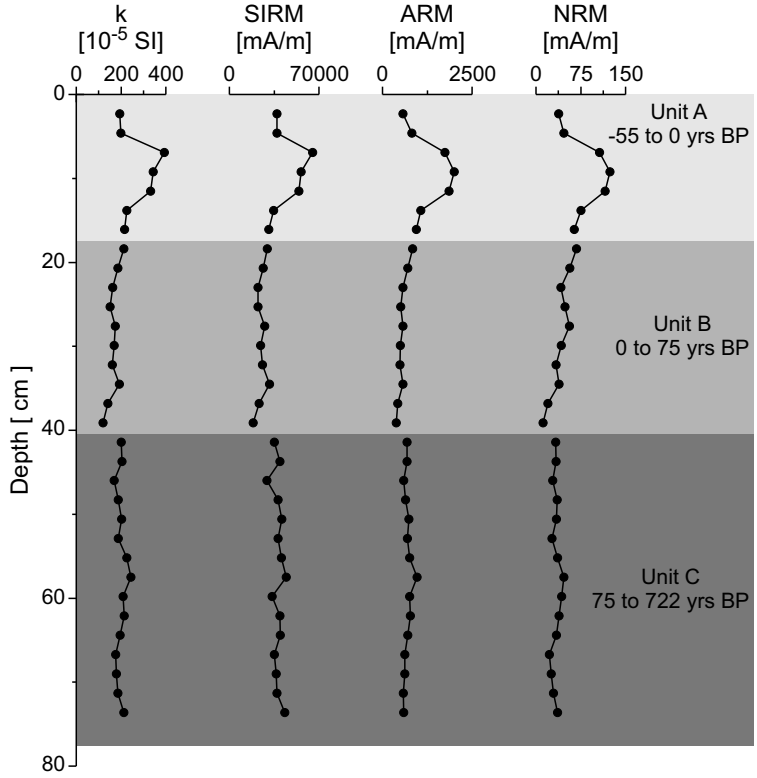

Fig. 3. Concentration-dependent parameters: magnetic susceptibility *k*, saturation isothermal remanent magnetization *SIRM*, anhysteretic remanent magnetization *ARM* and natural remanent magnetization *NRM* as a function of depth (age).

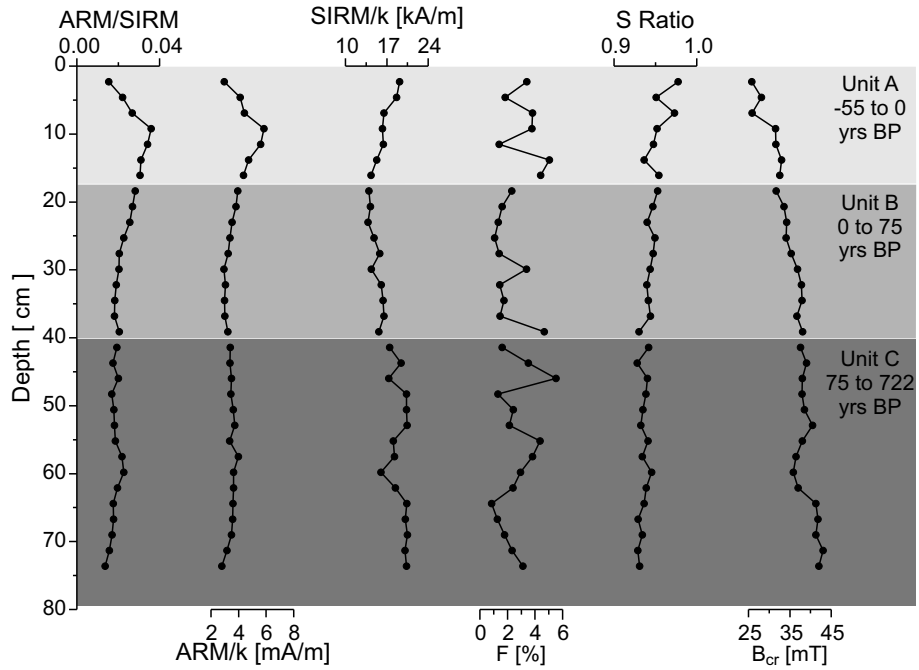

Fig. 4. Magnetic grain size parameters ($ARM/SIRM$, ARM/k , F), $SIRM/k$ and magnetic mineralogy estimators ($S = -IRM_{-300\,\mathrm{mT}}/SIRM$ and remanent coercive force B_{cr}) as a function of depth (age). *ARM*: anhysteretic remanent magnetization, *IRM*: isothermal remanent magnetization, *SIRM*: saturation remanent magnetization, *k*: magnetic susceptibility, *F*: relative frequency-dependent susceptibility, B_{cr}: remanent coercive force.

minerals at 9.2 cm (1978 AD), and is observed in all concentration-dependent parameters (*k*, *NRM*, *ARM*, *IRM*). The concentration change at 1978 AD is coeval with a sharp increase of inter-parametric ratios ($ARM/SIRM$ and ARM/k , Fig. 4). A slight decrease in the concentration parameters is observed at 39.1 cm (1876 AD) level and it represents the limit between lithological Units C and B where the sediments change from compact gray with low organic matter content to high organic matter percentages (*Guerra et al., 2015*).

F values are mostly below 4% (Fig. 4), which implies that super-paramagnetic grains are not important in the assemblages of magnetic grains (*Dunlop and Özdemir, 2007*). Variations in the magnetic grain size can be typically monitored by analysing inter-parametric ratios between concentration dependent parameters (*Turner, 1997*). $ARM/SIRM$ and ARM/k show high values for small magnetic particles and vice versa. Both proxies vary with similar amplitudes throughout the record (Fig. 4). In particular, the sector between 27.6 and 9.2 cm (1923–1978 AD) shows a slight trend towards finer magnetic grains, followed by a slight trend towards coarser magnetic grains during the last 30 years (Fig. 4).

Stepwise acquisition of *IRM* documents that 90% of the *SIRM* was acquired in fields of 200 mT for most samples (Fig. 5a). Progressive removal of *SIRM* indicates that B_{cr} varies approximately between 26 and 43 mT (decreasing from bottom to top) and the *S* ratio increase from 0.93 at bottom to 0.95 at the top of the core as seen in Fig. 4. These are typical values for magnetite-type minerals, in accordance with the graph of $SIRM/k$ vs. B_{cr} (Fig. 5b, *Peters and Dekkers, 2003*). *Peters and Dekkers (2003)* also indicate the possibility of finding maghemite with similar $SIRM/k$ and B_{cr} values. Plots of MDF_{ARM} and MDF_{NRM} vs. depth (Fig. 5c) show that both have a small range of variation, but the MDF_{ARM} values present a narrower range. The mean values for MDF_{NRM} and MDF_{ARM} are 12.5 and 16.9 mT, respectively. The plot of *SIRM* vs. *k* (*Thompson and Oldfield, 1986*, Fig. 5d) is useful for magnetic grain size estimation and magnetic concentration when the main carrier of the remanence is magnetite. Most of the samples from Units A and C (n = 19) are in the 2–4 μm region and 10 samples from Unit B, and 3 samples from Units A and C in the 4–8 μm region. Only three samples have concentration of magnetite >0.1% (1988 AD, 1978 AD and 1969 AD).

The shape of hysteresis loops (Fig. 6, upper part) is characteristic of magnetite. Furthermore, zero magnetization is reached during heating (Fig. 6, lower part) at or near the Curie temperature (T_C) of magnetite (580°C; *Dunlop and Özdemir, 1997, 2007*).

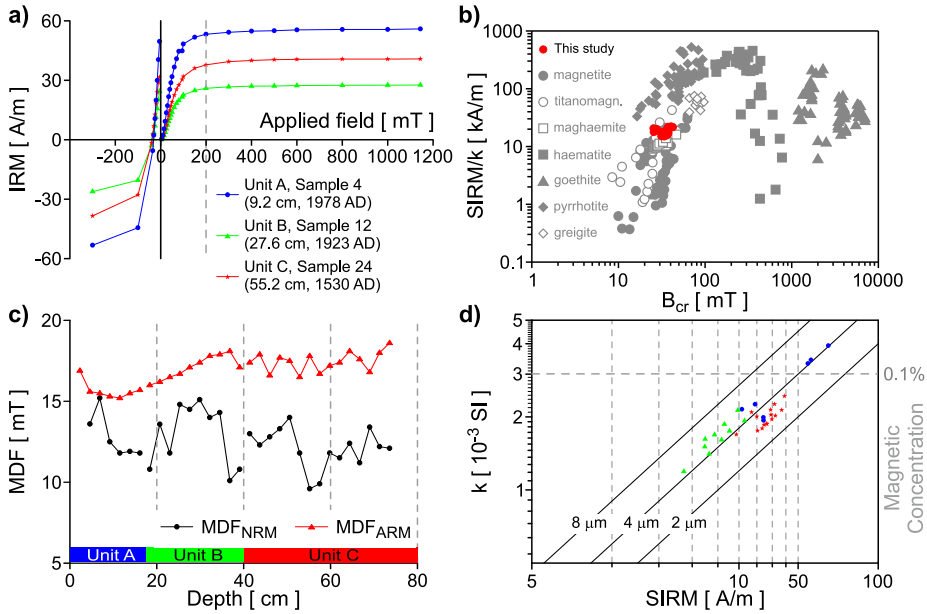

Fig. 5. Rock magnetic results obtained from remanent magnetization measurements. *IRM*: isothermal remanent magnetization, *SIRM*: saturation remanent magnetization, *k*: magnetic susceptibility, B_{cr}: remanent coercive force, *MDF*: median destructive field, *NRM*: natural remanent magnetization, *ARM*: anhysteretic remanent magnetization. The grey and white datapoints in b) are from *Peters and Dekkers (2003)*. (© Elsevier Ltd.)

Besides, a weak high temperature phase ($T_C > 580$°C) can be detected. In general, magnetization values are high in Unit C and low in Unit B, while samples from Unit A yielded middle magnetization values. This is the same behaviour we have already obtained for *k*, *ARM* and *SIRM*. The hysteresis curves show an increasing trend from 300 mT due to the presence of a low amount of paramagnetic minerals. Hysteresis ratios (Fig. 7) indicate that all samples belong to the pseudo-single-domain (PSD) region (*Day et al., 1977*; *Dunlop, 2002*). This is consistent with the symmetrical hysteresis cycles

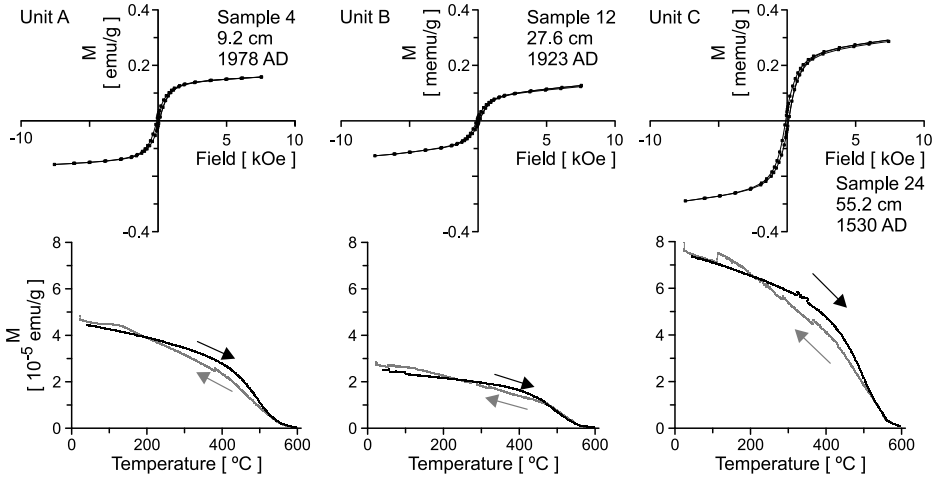

Fig. 6. Hysteresis curves (upper part) and temperature dependence of magnetization (lower part) for three selected samples, one for each lithological unit. *M*: magnetization.

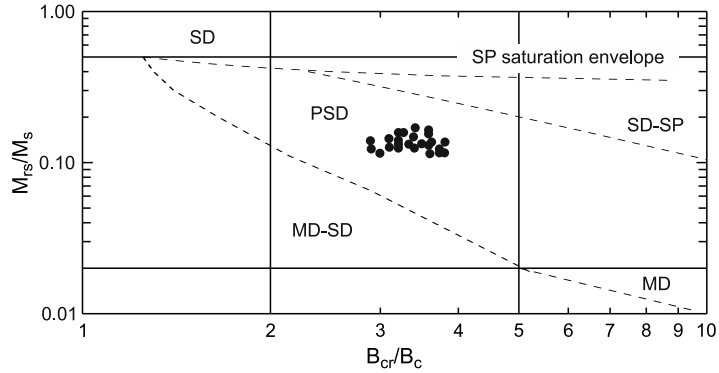

Fig. 7. Day Plot modified by *Dunlop (2002)* to estimate the domain state (SD: single-domain, PSD: pseudo-single-domain, MD: multi-domain, SP: super-paramagnetic) of magnetic carriers determined from hysteresis loops after dia and paramagnetic correction and back-field remanent remagnetization. M_{rs}: saturation remanent magnetization, M_S: saturation induced magnetization, B_{cr}: remanent coercive force, B_c: coercive force.

(calculated after dia and paramagnetic correction) pointing to the assemblages of PSD particles yielding quite similar values, near to the origin, without evidence of wasp-waisted behavior which probably reflects very restricted ranges of the opaque mineral coercivities (*Dunlop, 2002*).

4.3. Paleomagnetic analysis

The AF demagnetization results of representative samples are illustrated in Fig. 8. Most of the samples show no systematic change in the direction of their remanent magnetization during AF demagnetization but they show a small viscous magnetization, which could be easily removed by 5 mT AF demagnetization (Fig. 8, Sample 12). *NRM* intensities were almost completely demagnetized in fields of 60 mT (Fig. 8). The demagnetization data from 10 mT onwards show a stable behaviour, and a characteristic direction of the remanent magnetization can be calculated using principal component analysis (*Kirschvink, 1980*) with maximum angular deviations (*MAD*) lower than 10° for the samples of Units A and B. For samples from 20 to 27 cm (46 to 62 cm), it was difficult to estimate a reliable direction during the magnetic cleaning (Fig. 8) and *MAD* values are higher than 10° for some samples (Fig. 9).

Since the core was not orientated relative to magnetic north, the declination values are centred about average declination, and then this value was subtracted from the entire

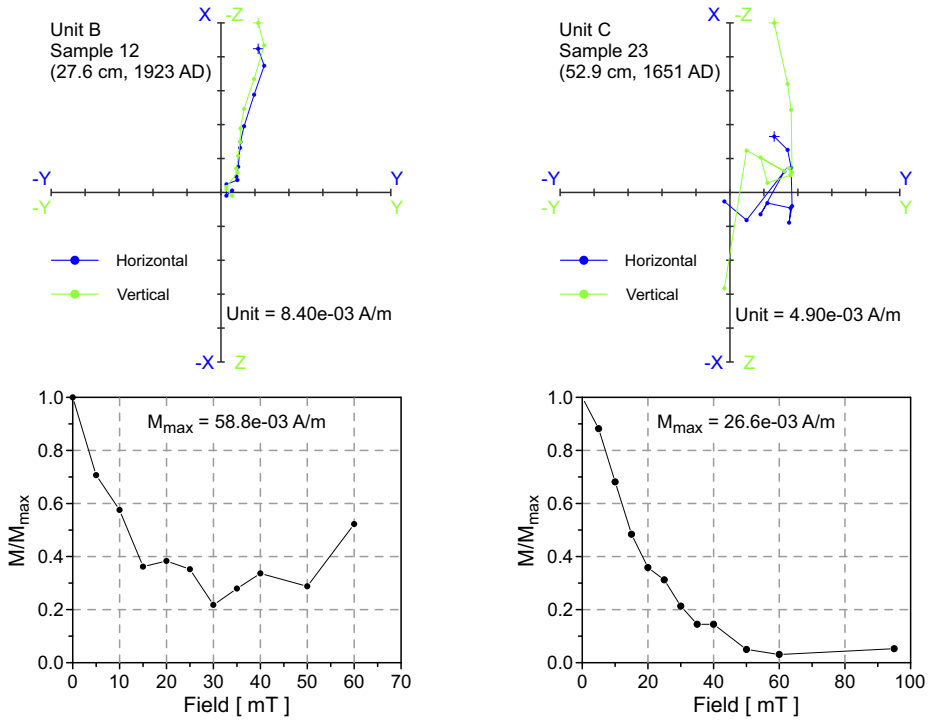

Fig. 8. Demagnetization curves for two representative samples. 75% of the samples behave as Sample 12, and the remaining 25% behave as Sample 23.

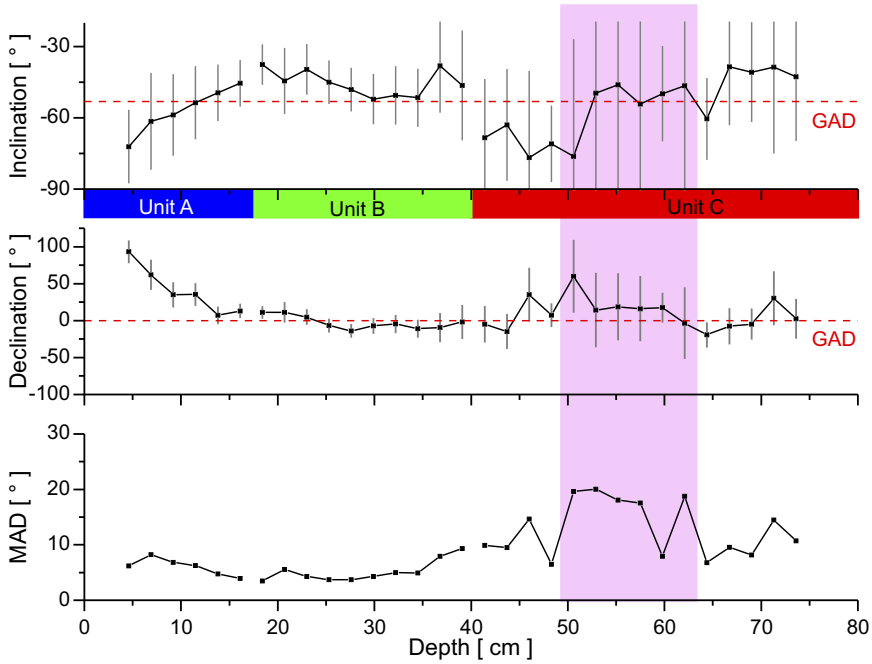

Fig. 9. Directional results of the geomagnetic field. Inclination, declination and the 95% confidence level (α_{95}, grey vertical bars) were calculated according to *Khokhlov and Hulot (2016)*. The shaded sector corresponds to samples with bad records of the directions and, as a consequence, high maximum angular deviation (*MAD*) values. In the inclination and declination records, the expected value of the geocentric axial dipole (GAD) is shown.

record to centre it around 0° (Fig. 9). According to the results shown in Fig. 9, the average inclination is −52° ± 11°, while the inclination of the geocentric axial dipole (GAD) at the coring site is −53°6′ (Fig. 9).

5. DISCUSSION

5.1. Climate variability: the historical record

Figure 10 shows the magnetic susceptibility record at the end of the LIA event (from 1860 to 1900 AD) compared with rainfall level for Buenos Aires city. This record shows a slight upward trend in rainfall from the mid-19-th century to the early 20-th century, coinciding with the end of the LIA and the establishment of current conditions, with significant climate variability. The k log shows an opposite behaviour to precipitation curve between 1861 and 1878 AD (slope of −0.6 mm/yr and correlation coefficient $r = 0.4$) consistent with a slight increase in magnetic grain size (decreasing trend in $SIRM/k$, Fig. 4) and a positive correlation between 1879 and 1900 AD (slope of 4.5 mm/yr, $r = 0.6$) when no variations in magnetic grain size are observed. The period of

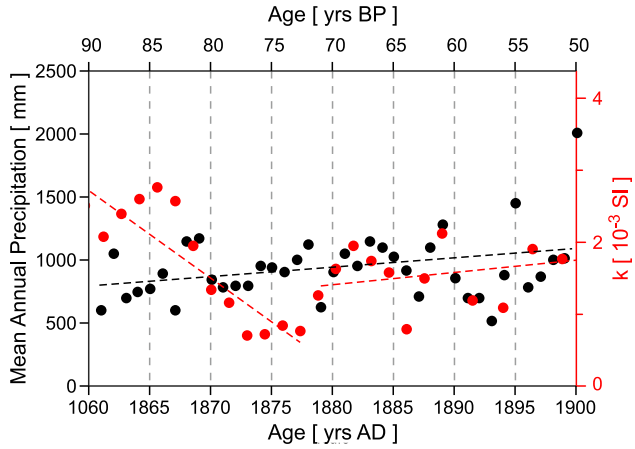

Fig. 10. Comparison of rainfall record during 1861–1900 in "Estancia los Yngleses" General Lavalle, Buenos Aires province (after *Deschamps et al., 2014*) with the magnetic susceptibility (*k*) data from core LMe.

1878–1879 could probably indicate the end of the LIA in Melincué region. Climate change evidences at 1880 were found by *Guerra et al. (2016)* as indication of a limit for the LIA.

Based on historical data and ostracods, *Laprida and Valero-Garcés (2009)* suggested three different climatic moments during historical times in the humid Pampa: the first one - between ca. 1480 and 1690 AD - corresponding to a predominantly wet period; the second one - between 1700 and 1850 AD - when the climate would have been drier than the current one; and finally the third stage with wetter conditions, which has been established since 1850. Coincidently, *Deschamps et al. (2014)* suggest an increase in annual rainfall of about 200 mm every 50 years from the mid-18-th century to the early 20-th century, with the establishment of wet conditions from mid-19-th century, coinciding with that indicated by *Laprida and Valero-Garcés (2009)* and also by *Deschamps et al. (2003)*. The dry and cold conditions correspond to the effects of the Little Ice Age (LIA), which would have affected the Pampas region more sharply in a short period of 150 years (1700–1850 AD). However, the LIA has been a global phenomenon, which started ca. 1300 AD and finished in 1870 AD (*de Menocal, 2001*). In Patagonia, Argentina, several authors indicate cold and wet conditions for the period 1540–1820 AD (*Haberzettl et al., 2005*, and references therein). In Peruvian ice cores wet conditions were found from 1500 to 1720 AD followed by dry conditions from 1720 to 1860 AD (*Thompson et al., 1985*) According to the information listed above from the Pampas, a coincidence between the dates of the end of the LIA and the end of the dry period is observed, but there are discrepancies in the starting dates. The reasons for the discrepancies could be that every proxy variation can be caused by several climate forcings and/or errors derived from the methods used to date the samples. In consequence, the extension and expression of the LIA event could be different in different environments.

5.2. Paleomagnetic and rock magnetic observations

Declination and inclination values for core LMe are generally consistent between consecutive samples and reveal gradually varying directional changes (Fig. 9). These changes appear to be unrelated to magnetic or non-magnetic variations in lithology, even for the sector 50–63 cm (1650–1270 AD) associated with high *MAD* values. An environmental influence appears likely, between 1300 and 1800 AD, where the climate was drier than the current one. An increase in the magnetic grain size is suggested by a decrease in the $SIRM/k$ record. This would indicate that the lake water level was low during this period and the sediment could be moved in a more energetic environment. In this period, the sediment in the coring site could be cover by water only circumstantially consistent with the increase in *MAD* values and the historical record of the area (*Deschamps et al., 2014*). Particularly, a fort was established around 1780 AD few meters from the coring site (personal communication, Museum of Melincué City) when the lake had a low water level. The fixing of the magnetization presumably occurs during consolidation, at a depth (known as the lock-in depth) where the porosity of the sediment decreases to the point that the particles are pinned (*Tauxe, 1998*). Because the core was collected near the shore, the dry conditions could have affected the area so the sediment was unconsolidated and presumably slightly moved by waves from its original position.

Due to the lack of paleosecular variations records in the studied area, the data of Laguna Melincué were compared with the GUFM1 model (*Jackson et al., 2000*) and models of the family of spherical harmonic geomagnetic models (*Korte and Constable, 2011*; *Korte et al., 2011*), which includes Cals3k.3, Cals3k.3b, Cals3k.4a and Cals3k.4b and Cals10k.1b models (based on all sources of paleomagnetic data). In particular, GUFM1 and Cals3k.4 (*Korte and Constable, 2011*) reproduce, albeit with some differences in amplitude, the PSV recorded in Laguna Melincué (Fig. 11). Inclination values are shallower and deeper than model predictions from 1228 to 1263 AD and from 1870 to 1990 AD, respectively and from 1272 to 1655 AD they show a very good agreement. From 1590 to 1620 AD the models have opposite behaviours but no data is available from our record to define the trend. The biggest discrepancy is observed in the period 1655–1870 AD, although it is necessary to note that there are only three values

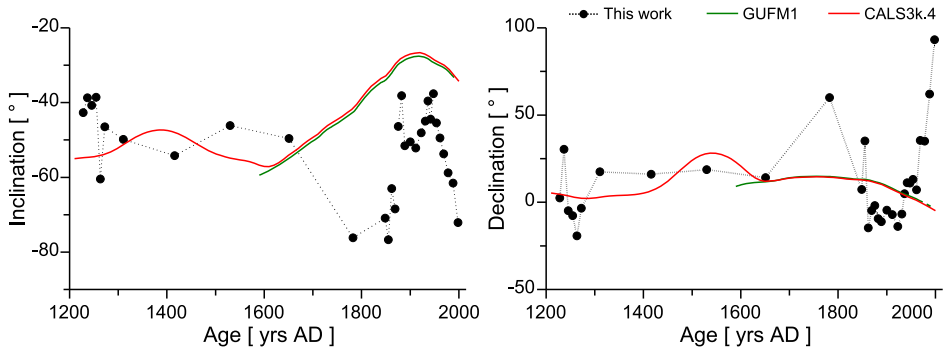

Fig. 11. Inclination and declination curves obtained in this work, compared with the GUFM1 (*Jackson et al., 2000*) and Cals3k.4 (*Korte and Constable, 2011*) models.

from this work. A similar analysis could be performed for declination record, indicating two possible explanations. The first possibility is that the extreme dry conditions observed in the period between 1700 and 1850 AD affected the inclination/declination values. The other option is that the models GUFM1 and CAL3k.4 do not sufficiently reproduce non-dipolar local features. More studies would be necessary to elucidate this question.

The mean paleomagnetic inclination for core LMe (–52.2°) show a quite good agreement with the expected inclination at the studied site (–53.1°) for a geocentric axial dipole (GAD) field. This finding further supports the quality of the results.

The rock magnetic analyses were conducted to investigate three aspects of the magnetic signal, the concentration of magnetic minerals, the magnetic grain size of the sediment and the variations in the magnetic mineralogy.

The remanences follow the same behaviour as k (Fig. 3), suggesting that they are mostly influenced by changes in concentration of magnetic minerals. $ARM/SIRM$ and ARM/k (Fig. 4) suggest that the magnetic grain size has small variations from bottom to approximately 1911 AD. Afterwards, magnetic grain size shows significant decrease ($ARM/SIRM$ and ARM/k increase) until 1978 AD and it has become coarser since then. High organic matter content in Unit A at these ages was already described by *Guerra et al. (2015)*. The high in organic matter and the variations in magnetic grain size could be associated with dissolution of magnetic particles. Dissolution of detritic magnetic minerals has been observed in marine and lake sediments deposited during warm periods due to the high content of organic matter (*Gogorza et al., 2011*). Dissolution tends preferentially to remove more fine-grained than coarse grained magnetic particles because of their higher surface area-to-volume ratios (*Franke et al., 2004*).

Altogether the rock magnetic studies (temperature-dependent magnetization, step-wise acquisition of *IRM* in field up to 1.2 T, *S* ratio, the shape of the hysteresis loop, *MDF* of *NRM* and *ARM*, and B_{cr}) clearly identified magnetite PSD as the dominant magnetic carrier.

6. CONCLUSIONS

Rock magnetic studies suggest the presence of ferrimagnetic minerals with PSD (titano) magnetite as main magnetic carrier of the remanent magnetization. According to the correlation with the susceptibility vs. age curves of *Guerra et al. (2015)*, our record spans approximately the last 720 years.

The changes observed in concentration of magnetic grains indicate different climatic environments while the magnetic grain size variations suggest periods of high and low lake level. Particularly, magnetic susceptibility seems to be a good proxy to estimate paleoprecipitations in combination with changes in magnetic mineralogy and grain size. And with information of historical data a model for paleolake level variations could be achieved.

A stable, primary remanent magnetization was retrieved from most of studied samples. The well-defined changes in magnetic parameters (directional and non-directional data) indicate the potential of this lake for paleomagnetic studies.

The paleodirectional record obtained for the Laguna Melincué agrees well with Cals3k.3 model except for the dry period probably due to the fact that the core was extracted near the shore.

Acknowledgements: We are much indebted to Ministerio de Educación de la República Argentina - Secretaría de Políticas Universitarias. Programa REDES VII of Secretaría de Políticas Universitarias (SPU) de la República Argentina and Agencia Nacional de Promoción Científica y Tecnológica (ANPCyT) PICTO-2010 Nº0096. A. Goguitchaichvili acknowledges the partial financial support given by UNAM-PAPIIT Project IN105214. The authors want to thank to the two anonymous reviewers for their useful comments. The authors also want to thank to Andrew Jackson for his help with the data of GUFM1 model.

References

Anderson N.J. and Rippey B., 1988. Diagenesis of magnetic minerals in the recent sediments of a eutrophic lake. *Limnol. Oceanogr.*, **33**, 1476–1492.

Bartington Instruments Ltd., 1994. *Environmental Magnetic Susceptibility-Using the Bartington MS2 System*. Operation Manual, Bartington Instruments Ltd., Witney, U.K.

Biasatti N., Delannoy L., Peralta E., Pire E., Romano M. and Torres G., 1999. *Cuenca Hidrográfica del Humedal de la Laguna Melincué, Provincia de Santa Fe*. ProDIA, SRNyDS, Buenos Aires, Argentina (in Spanish).

Bloemendal J., King J.W., Hall F.R. and Doh S.J., 1992. Rock magnetism of late Neogene and Pleistocene deep-sea sediments: Relationship to sediment source, diagenetic processes, and sediment lithology. *J. Geophys. Res.*, **97**, 4361–4375, DOI: 10.1029/91JB03068.

Brunetto E., Iriondo M., Zamboni L. and Gottardi G., 2010. Quaternary deformation around the Palo Negro area, Pampa Norte, Argentina. *J. South Am. Earth Sci.*, **29**, 627–641.

Bruniard E.D., 1982. La diagonal árida Argentina: un límite climático real. *Revista Geográfica*, **95**, 5–20 (in Spanish).

Chaparro M.A.E., Gargiulo J.D., Irurzun M.A., Chaparro M.A.E., Lecomte K.L., Böhnel H.N., Córdoba F.E., Vignoni P., Manograsso Czalbowski N.T., Lirio J.M., Nowaczyk N.R., Sinito A.M., 2014. El uso de parámetros magnéticos en estudios paleolimnológicos en Antártida. *Latin American Journal of Sedimentology and Basin Analysis*, **21(2)**, 77–96 (in Spanish).

Day R., Fuller M. and Schmidt V.A., 1977. Hysteresis properties of titanomagnetites: Grain size and composition dependence. *Phys. Earth Planet. Inter.*, **13**, 260–267.

de Menocal P.B., 2001. Cultural responses to climate change during the late Holocene. *Science*, **292**, 667–673.

Dearing J., Dann R., Hay K., Lees J., Loveland P., Maher B. and O'Grady K., 1996. Frequency-dependent susceptibility measurements of environmental materials. *Geophys. J. Int.*, **124**, 228–240.

Deschamps J.R., Otero O. and Tonni E.P., 2003 *Cambio climático en la pampa bonaerense: las precipitaciones desde los siglos XVIII al XX*. Documentos de Trabajo, Universidad de Belgrano, Área de estudios agrarios 109, Buenos Aires, Argentina, 1–18 (in Spanish).

Deschamps J.R., Otero O. and Tonni E.P., 2014. *Las precipitaciones en el noreste de la región pampeana (Provincia de Buenos Aires, Argentina) entre 1745-1900. Una reconstrucción histórica*. Documentos de Trabajo 304. Universidad de Belgrano, Área de estudios agrarios 109, Buenos Aires, Argentina, 1–18 (in Spanish) 1-18.

Dunlop D.J., 2002. Theory and application of the Day plot (Mrs/Ms versus Hcr/Hc). 1. Theoretical curves and tests using titanomagnetite data. *J. Geophys. Res*., **107(B3)**, 2056.

Dunlop D.J. and Özdemir Ö., 1997. *Rock Magnetism: Fundamentals and Frontiers*. Cambridge University Press, Cambridge, U.K.

Dunlop D.J. and Özdemir O., 2007. Magnetisations in rocks and minerals. In: Kono M. (Ed.), *Geomagnetism*. Treatise on Geophysics **5**, Elsevier, Amsterdam, The Netherlands, 277–336.

Franke C., Hofmann D. and von Dobeneck T., 2004. Does lithology influence relative paleointensity records? A statistical analysis on South Atlantic pelagic sediments. *Phys. Earth Planet. Inter.*, **147**, 285–296.

Gogorza C.S.G., Sinito A.M., Ohlendorf C., Kastner S. and Zolitschka B., 2011. Paleosecular variation and paleointensity records for the last millennium from southern South America (Laguna Potrok Aike, Santa Cruz, Argentina). *Phys. Earth Planet. Inter.*, **184**, 41–50.

Guerra L., Piovano E., Córdoba F., Sylvestre F. and Damatto S., 2015. The hydrological and environmental evolution of shallow Lake Melincué, central Argentinean Pampas, during the last millennium. *J. Hydrol.*, **529**, 570–583.

Guerra L., Piovano E.L., Córdoba F.E., Tachikawa K., Rostek F., Garcia M., Bard E. and Sylvestre F., 2016. Climate change evidences from the end of the Little Ice Age to the Current Warm Period registered by Melincué Lake (Northern Pampas, Argentina). *Quat. Int.*, DOI: 10.1016/j.quaint.2016.06.033 (in press).

Haberzettl T., Fey M., Lucke A., Maidana N., Mayr C., Ohlendorf C., Schabitz F., Schleser G.H., Wille M. and Zolitschka B., 2005. Climatically induced lake level changes during the last two millennia as reflected in sediments of Laguna Potrok Aike, southern Patagonia (Santa Cruz, Argentina). *J. Paleolimnol*., **33**, 283–302.

Irurzun M.A., Gogorza C.S.G., Sinito A.M., Chaparro M.A.E., Prieto A., Laprida C., Lirio J.M., Navas A.M. and Nuñez H., 2014a. A High-Resolution Palaeoclimate Record for the Last 4800 cal. years BP on Lake La Brava SE Pampas Plains, Argentina. *Geofis. Int.*, **53**, 365–383.

Irurzun M.A., González Bonorino G., Gogorza C.S.G., Hall S., Abascal L., Alonso R.N. and Larcher N., 2014b. Caracterización magnética y datación preliminar mediante paleointensidades relativas de sedimentos lacustres de la formación Tajamar (Guachipas), Salta, Argentina. *Latinmag Letters*, **4**, LL14-0404Rs (in Spanish).

Irurzun M.A., Orgeira M.J., Gogorza C.S.G., Sinito A.M., Campagnucci R. and Zolitschka B., 2014c. Magnetic parameters and their palaeoclimatic implications - the sediment record of the last 15,500 cal. BP from Laguna Potrok Aike (Argentina). *Geophys. J. Int.*, **198**, 710–726.

Jackson A., Jonkers A.R.T. and Walker M.R., 2000. Four centuries of geomagnetic secular variation from historical records. *Phil. Trans. R. Soc. London A*, **358**, 957–990.

Khokhlov A. and Hulot G., 2016. Principal component analysis of palaeomagnetic directions: converting a Maximum Angular Deviation (MAD) into an α_{95} angle. *Geophys. J. Int.*, **204**, 274–291

Kirschvink J.L., 1980, The least squares line and plane and the analysis of paleomagnetic data. *Geophys. J. R. Astron. Soc.*, **62**, 699–718.

Korte M. and Constable C., 2011. Improving geomagnetic field reconstructions for 0–3 ka. *Phys. Earth Planet. Inter.*, **188**, 247–259.

Korte M., Constable C., Donadini F. and Holme R., 2011. Reconstructing the Holocene geomagnetic field. *Earth Planet. Sci. Lett.*, **312**, 497–505.

Laprida C., Orgeira M.J. and García Chapori N., 2009. El registro de la Pequeña Edad de Hielo en lagunas pampeanas. *Rev. Asoc. Geol. Argentina*, **65**, 603–611 (in Spanish).

Laprida C. and Valero Garcés B., 2009. Cambios ambientales de épocas históricas en la pampa bonaerense en base a ostrácodos: historia hidrológica de la laguna de Chascomús. *Ameghiniana*, **46**, 95–111 (in Spanish).

Lisé-Pronovost A., St-Onge G., Gogorza C., Haberzettl T., Preda M., Francus P., Zolitschka B. and the PASADO Science Team, 2013. High-resolution paleomagnetic secular variation and relative paleointensity since the Late Pleistocene in Southern South America. *Quat. Sci. Rev.*, **71**, 91–108.

Liu Q., Roberts A.P., Larrasoaña J.C., Banerjee S.K., Guyodo Y., Tauxe L. and Oldfield F., 2012. Environmental magnetism: principles and applications. *Rev. Geophys.*, **50**, RG4002, DOI: 10.1029/2012RG000393.

Lund S.P. and Platzman E., 2016. Paleomagnetic chronostratigraphy of late Holocene Zaca Lake, California. *The Holocene*, **26**, 814–821.

Moernaut J., Verschuren D., Charlet F., Kristen I., Fagot M. and De Batist M., 2010. The seismic-stratigraphic record of lake-level fluctuations in Lake Challa: Hydrological stability and change in equatorial East Africa over the last 140 kyr. *Earth Planet. Sci. Lett.*, **290**, 214–223.

Pasotti P., Albert O. and Canoba C., 1984. *Contribución al conocimiento de la laguna Melincué*. Facultad de Ciencias Exactas e Ingeniería, Universidad Nacional de Rosario, Rosario, Argentina, 31 pp. (in Spanish).

Peralta E., 2003. *Propuesta para la planificación del manejo sustentable de la cuenca hidrográfica y de aporte directo de la Laguna Melincué*. Reporte Técnico RT-ID-03/005. Facultad de Ciencias Exactas, Ingeniería y Agrimensura de la Universidad Nacional de Rosario, Rosario, Argentina, 15 pp. (in Spanish).

Peters C. and Dekkers M.J., 2003. Selected room temperature magnetic parameters as a function of mineralogy, concentration and grain size. *Phys. Chem. Earth*, **28**, 659–667.

Piovano E.L., Larizzatti F.E., Fávaro D.I., Oliveira S.M., Damatto S.R., Mazzilli B.P. and Ariztegui D., 2004. Geochemical response of a closed-lake basin to 20th century recurring droughts/wet intervals in the subtropical Pampean Plains of South America. *J. Limnol.*, **63**, 21–32.

Šroubek P., Diehl J.F. and Kadlec J., 2007. Historical climatic record from flood sediments deposited in the interior of Spirálka Cave, Czech Republic. *Paleogeogr. Paleoclimatol. Paleoecol.*, **251**, 547–562.

Tauxe L., 1993. Sedimentary records of relative paleointensities of the geomagnetic field: theory and practice. *Rev. Geophys.*, **31**, 319–354.

Tauxe L, 1998. *Paleomagnetic Principles and Practice*. Kluwer Academic Publishers, New York.

Tauxe L., Mullender T.A.T. and Pick T., 1996. Potbellies, wasp-waists, and superparamagnetism in magnetic hysteresis. *J. Geophys. Res.*, **101(B1)**, 571–583.

Thompson R. and Oldfield F., 1986. *Environmental Magnetism*. Allen & Unwin, London, U.K.

Turner G.M., 1997. Environmental magnetism and magnetic correlation of high resolution lake sediment records from Nortern Hawke's Bay, New Zealand. *N. Z. J. Geol. Geophys*., **40**, 287–298.

Veski S., Seppa H. and Ojala A.E.K., 2004. Cold event at 8200 yr B.P. recorded in annually laminated lake sediments in eastern Europe. *Geology*, **32**, 681–684.

Yang S., Odah H. and Shaw J., 2000. Variations in the geomagnetic dipole moment over the last 12,000 years. *Geophys. J. Int.*, **140**, 158–162.